Comparative CmFD Study on Geometric and Algebraic Coupled Level Set and Volume of Fluid Methods

Orkodip Mookherjee, Shantanu Pramanik, and Atul Sharma

1 Introduction

Computational multi-Fluid Dynamics (CmFD) is a branch of Computational Fluid Dynamics (CFD) which involves a study on multi-physics fluid dynamics, heat transfer, and phase change processes occurring among multiple fluids. For the CmFD, accurate prediction of the interface plays a vital role in simulating a variety of two-phase phenomena like droplet breakup and coalescence, droplet evaporation, droplet combustion, spray atomization, etc. As compared to CFD for a single phase flow, CmFD for two-phase flow involves additional challenges on the discontinuity of material properties across the interface and mass, momentum, and energy transport at the interface. Various CmFD methods have been developed to address these challenges which can be broadly classified as Lagrangian and Eulerian methods. The present work deals with the Eulerian approach, which involves capturing the interface on a fixed mesh. Common Eulerian methods are Volume Of Fluid (VOF) method [4], Level Set (LS) method [14], and Coupled Level Set and Volume Of Fluid (CLSVOF) method [13].

In CLSVOF method, the interface is represented by a level set function ϕ and the conservation of mass is guaranteed by a volume fraction field F. The key role of any VOF-type scheme is the numerical approximation of the advection fluxes to update the fluid volume fractions. Based on the computation of fluxes, there are two types of VOF method: algebraic and geometric methods. An algebraic VOF method, like that of Hirt and Nichols [4], does not require any explicit geometrical reconstruction of the interface in the solution procedure. Thus, these VOF methods are quite straightforward and easy to implement. A geometric VOF method, on the other hand, consists

O. Mookherjee (✉) · S. Pramanik
Department of Mechanical Engineering, NIT Durgapur, Durgapur 713209, India
e-mail: om.18me1101@phd.nitdgp.ac.in

A. Sharma
Department of Mechanical Engineering, IIT Bombay, Mumbai 400076, India

K. M. Singh et al. (eds.), *Fluid Mechanics and Fluid Power, Volume 5*, Lecture Notes in Mechanical Engineering, https://doi.org/10.1007/978-981-99-6074-3_1

of two steps: advecting the interface, and, identifying its new position (geometrical reconstruction). These features make the computational implementation reasonably complex; the complexity increases further for 3D problems.

An overall comparison between algebraic VOF methods [10] and geometric VOF methods reveal that the results obtained from algebraic methods are better than Simple Line Interface Calculation (SLIC) VOF method but inferior to most of the Piecewise Linear Interface Calculation (PLIC) VOF methods [8]; particularly for complex flow fields. However, development of new algebraic interface capturing methods are justified because they are relatively much simpler and robust than a PLIC type VOF scheme.

An algebraic interface capturing scheme using the hyperbolic tangent function, Tangent of the Hyperbola for INterface Capturing (THINC) was first developed by Xiao et al. [15]. The smooth step-like nature of the hyperbolic tangent function makes it suitable for interpolating the advection fluxes of the volume fraction field and is effective in eliminating numerical diffusion and oscillations. Numerical experiments [16] reveal that the THINC scheme coupled with the Weighted Line Interface Calculation (WLIC) framework possesses adequate accuracy and has a more robust performance as compared to existing high-resolution scheme-based algebraic methods.

Considering the advantages and disadvantages of algebraic and geometric type of CLSVOF methods, a direct comparison between them on a variety of multiphase flow problems is not available in the present literature. Therefore, the objective of this work is to present a numerical methodology of the PLIC-based geometric CLSVOF and WLIC-THINC scheme-based algebraic CLSVOF methods along with the incompressible Navier–Stokes equations on a co-located grid using the balanced-force approach. An in-house code is developed and performance of both the numerical techniques are studied on standard CmFD benchmark problems like dam break and bubble rise.

2 Governing Equations

The present work considers two different fluids, separated by an interface, and each fluid is assumed to be incompressible and immiscible. A single fluid formulation is used, where the same set of mass and momentum conservation equations are used for both the fluids. To capture the interface, CLSVOF method requires solution of separate advection equations for the level set field ϕ and volume fraction field F. The advection equations are given as,

$$\frac{\partial \Gamma}{\partial t} + \nabla \cdot (\boldsymbol{u}\Gamma) - \Gamma \nabla \cdot \boldsymbol{u} = 0 \tag{1}$$

where $\Gamma = \phi$ for level set advection equation and $\Gamma = \chi$, a characteristic function, for advection of volume fraction field. The volume fraction F_P is defined as the cell averaged value of χ given as,

$$F_P = \overline{\chi}_P = \frac{1}{\Delta x \Delta y} \int_{x_w}^{x_e} \int_{y_s}^{y_n} \chi \, \mathrm{d}x \mathrm{d}y \tag{2}$$

The mass and momentum conservation equations are given as

$$\nabla \cdot \boldsymbol{u} = 0 \tag{3}$$

$$\frac{\partial(\rho \boldsymbol{u})}{\partial t} + \nabla \cdot (\rho \boldsymbol{u}\boldsymbol{u}) = -\nabla p + 2\nabla \cdot [\mu \boldsymbol{D}] + \rho \boldsymbol{g} + \sigma k \nabla F \tag{4}$$

where $\boldsymbol{u}$ is the velocity vector, ρ is the density, μ is the viscosity, p is the hydrodynamic pressure, $\boldsymbol{g}$ is the acceleration due to gravity, σ is the surface tension coefficient, k is the curvature of the interface, and $\boldsymbol{D}$ is the rate of deformation tensor defined as $\left(\nabla \boldsymbol{u} + \nabla \boldsymbol{u}^T\right)/2$.

Following the work of Hong and Walker [5], a piezometric pressure P is defined as

$$P = p - \rho \boldsymbol{g} \cdot \boldsymbol{x} \tag{5}$$

Implementing this in Eq. 4, the modified Navier–Stokes equation is given as

$$\frac{\partial(\rho \boldsymbol{u})}{\partial t} + \nabla \cdot (\rho \boldsymbol{u}\boldsymbol{u}) = -\nabla P + 2\nabla \cdot [\mu \boldsymbol{D}] + \{(\rho_0 - \rho_1)\boldsymbol{g} \cdot \boldsymbol{x} + \sigma k\} \nabla F \tag{6}$$

Due to the piezometric formulation, the pressure and gravity forces appear as gradient quantities and can be treated identically in the discrete level. This treatment allows a perfect force balance between them in the scenarios where they are competing against each other. The fluid properties are represented as a function of volume fraction given by

$$\rho = \rho_1 F + \rho_0 (1 - F), \tag{7}$$

$$\mu = \mu_1 F + \mu_0 (1 - F) \tag{8}$$

where the subscripts 1 and 0 represent fluid 1 and 0, respectively.

3 Numerical Methodology

Finite volume method is used to discretize the governing equations, presented in Sect. 2. A co-located grid arrangement is followed, where all the solution variables (velocity, pressure, volume fraction, and level set) are defined at the centroid of each control volume (cell).

3.1 CLSVOF Advection Equations

The generalized CLSVOF advection equation (Eq. 1) is discretized using an operator splitting algorithm [13], given as

$$\overline{\Gamma}_P^* = \overline{\Gamma}_P^n - \frac{G_{xe}^n - G_{xw}^n}{\Delta x}\Delta t + \overline{\Gamma}_P^* \frac{u_e - u_w}{\Delta x}\Delta t, \tag{9}$$

$$\overline{\Gamma}_P^{n+1} = \overline{\Gamma}_P^* - \frac{G_{yn}^* - G_{ys}^*}{\Delta y}\Delta t + \overline{\Gamma}_P^* \frac{v_n - v_s}{\Delta y}\Delta t \tag{10}$$

The flux for the volume fraction advection equation in the x direction G_{xe} is given as

$$G_{xe} = -\int_{y_s}^{y_n}\int_{x_e}^{x_e - u_e\Delta t} \chi_{P_{\text{up}}}(x, y)\mathrm{d}x\mathrm{d}y \tag{11}$$

where P_{up} is defined as

$$P_{\text{up}} = \begin{cases} P \text{ if } u_e \geq 0 \\ E \text{ if } u_e < 0 \end{cases} \tag{12}$$

Similarly advection fluxes in the y direction can be obtained. For the level set advection equation, a second-order ENO scheme [14] is used to determine the advection fluxes. Finally, Strang-splitting [13] is employed to minimize the error by dimensional splitting.

For the PLIC-CLSVOF method, the characteristic function (χ) for the volume fractions is the sharp unit Heaviside function given as

$$\chi(x, y) = \begin{cases} 1 \text{ for fluid 1 at the point } (x, y) \\ 0 \text{ for fluid 1 at the point } (x, y) \end{cases} \tag{13}$$

A piecewise linear segment is geometrically constructed which defines the interface between the two fluids. The orientation and position of the interface are determined by the normal vector (calculated from the smooth level set field) and the volume fraction field, respectively. The advection fluxes are obtained by calculating the area under the linear interface segment. A detailed description of the method is presented in the literature [12, 13].

For the THINC-CLSVOF method, a hyperbolic tangent function is used as the characteristic function; given as

$$\chi_{xP} = \frac{1}{2}\left[1 + \alpha_x \tanh\left\{\beta\left(\frac{x - x_w}{\Delta x} - \tilde{x}_P\right)\right\}\right] \tag{14}$$

where α_x represents the direction of the interface; given as

$$\alpha_x = \begin{cases} 1 \text{ if } n_{xp} \geq 0 \\ -1 \text{ if } n_{xp} < 0 \end{cases} \tag{15}$$

where $\boldsymbol{n}$ is the interface normal and β is a smoothness parameter for the characteristic function. A larger value of β results in a sharp function thereby reducing the thickness of the diffused interface. In the present work, $\beta = 2.3$ which corresponds to three mesh smoothing. Further, $\tilde{x}_P \Delta x$ is the distance between x_w and the interface, indicating position of the interface in a two-fluid cell. The value of $\tilde{x}_P$ can be obtained from the cell volume fraction as

$$F_P^n = \frac{1}{\Delta x}\int_{x_w}^{x_e} \chi_P(x, \tilde{x}_P)\mathrm{d}x \tag{16}$$

By using such a smoothened characteristic function χ, the volume fraction field F becomes smoother than that of the PLIC-CLSVOF method. This feature is useful for the implementation of interfacial body forces in a continuum framework. Also, interface reconstruction is not required because the fluxes for volume fraction advection equation can be directly obtained by analytically integrating χ_x within the required limits. The accuracy of the present THINC-based algebraic method is further improved by coupling it with a WLIC framework, where the shape of the interface is weighted by using the weights calculated from the interface normal $\boldsymbol{n}$ given as,

$$\chi_P = \omega_{xP}(\boldsymbol{n}_P)\chi_{xp} + \omega_{yP}(\boldsymbol{n}_P)\chi_{yp} \tag{17}$$

where

$$\omega_{iP} = \frac{|n_{iP}|}{|n_{xP}| + |n_{yP}|} \tag{18}$$

are the weights, and χ_x and χ_y are the characteristic functions of the vertical and horizontal interface, respectively. n_x and n_y are the x and y component of the interface normal $\boldsymbol{n}$. Further details are available in [16].

After the solution of level set advection equation, the level set field is reinitialized to preserve it as the signed distance function. This is achieved by solving an Eikonal equation, given as

$$|\nabla\phi| = 1 \tag{19}$$

where the above equation is solved by using a fast sweeping method [18].

3.2 Navier–Stokes Equations

The Navier–Stokes equation is solved using a semi-explicit projection method, wherein the pressure and interfacial body force terms are considered implicitly with all other terms as explicit. The discretized momentum equation is given as

$$\begin{aligned}\frac{(\rho\boldsymbol{u})_P^{n+1} - (\rho\boldsymbol{u})_P^n}{\Delta t} &= -\nabla\cdot(\rho\boldsymbol{u}\boldsymbol{u})^n - \nabla P^{n+1} \\ &\quad + \nabla\cdot(2\mu\boldsymbol{D})^n + \{(\rho_0-\rho_1)\boldsymbol{g}\cdot\boldsymbol{x} + \sigma k\}\nabla F^{n+1}\end{aligned} \tag{20}$$

In the predictor step of the pressure projection method, the pressure and body force terms are not considered in the momentum equation; and the predicted cell center velocity $\boldsymbol{u}_P^*$ is given as

$$\rho\frac{\boldsymbol{u}_P^* - \boldsymbol{u}_P^n}{\Delta t} + \nabla\cdot(\rho\boldsymbol{u}\boldsymbol{u})^n = \nabla\cdot(2\mu\boldsymbol{D})^n \tag{21}$$

Momentum advection of the interfacial cells is achieved by the product of volume fraction-based advected mass and corresponding velocity at the donor cell face [1].

Subtracting Eq. (21) from Eq. (20), the corrected cell center velocity $\boldsymbol{u}_P^{n+1}$ is given as

$$\rho\frac{\boldsymbol{u}_P^{n+1} - \boldsymbol{u}_P^*}{\Delta t} = -\nabla P^{n+1} + \{(\rho_0-\rho_1)\boldsymbol{g}\cdot\boldsymbol{x} + \sigma k\}\nabla \mathrm{F}^{\mathrm{n+1}} \tag{22}$$

A proper balance between the interfacial and pressure forces in the co-located grid arrangement is achieved by using a balanced-force method [2]. The pressure field for the next time step is obtained from the pressure Poisson equation, which is derived from the divergence of Eq. (22) utilizing the continuity equation (Eq. 3); given as

$$\nabla \cdot \left(\frac{\Delta t}{\rho} \nabla P \right)^{n+1} = \nabla \cdot \left[\mathbf{u}^* + \frac{\Delta t}{\rho^{n+1}} \{(\rho_0 - \rho_1)\boldsymbol{g} \cdot \boldsymbol{x} + \sigma k\} \nabla F^{n+1} \right] \tag{23}$$

3.3 Solution Algorithm

A generalized solution algorithm for the present algebraic and geometric CLSVOF methods is presented as follows.

1. Initialize the velocity, pressure, volume fraction, and level set fields.
2. Calculate the geometric properties of the interface (normal and curvature).
3. Solve the prediction equation (Eq. 21) for the predicted velocity $\boldsymbol{u}_P^*$ at the cell centers.
4. Solve the pressure Poisson equation (Eq. 23) for the pressure field P.
5. Solve the correction equation (Eq. 22) for the final velocity $\boldsymbol{u}_P^{n+1}$ at the cell centers.
6. Advect the interface by solving the advection equations for the characteristic function χ and level set function ϕ.
7. Reinitialize the level set field.
8. Stop the simulations if the termination criteria is satisfied, or else repeat the process from step 2.

Computationally, the most expensive step in the above algorithm is solution of the pressure Poisson equation which is solved using a preconditioned GMRES method [11].

4 Results and Discussion

For a relative performance study of the present PLIC-CLSVOF and WLIC-THINC-CLSVOF methods, static droplet test for the surface tension model, and two sufficiently different benchmark CmFD problems on dam-break simulation and bubble rise are considered. In the dam-break problem involving collapse of a liquid column, gravitational force plays the dominating role. Contrarily, in the bubble rise problem, both the capillary and gravitational forces dictate the shape of the rising bubble.

4.1 Static Droplet

To compare the performance of the surface tension model, standard benchmark test of a static drop in equilibrium without any external forces is considered. Parameters of the test problem are same as that of Francois et al. [2]. The computational domain is a

Table 1 Magnitude of maximum spurious velocities $|u_{\max}|$ obtained after one and 50 time steps. The density ratio is 10 and the time step is 10^{-3}

T	PLIC	WLIC-THINC	Francois et al
Δt	6.4×10^{-3}	9.6×10^{-3}	4.87×10^{-3}
$50\Delta t$	1.38×10^{-1}	2.73×10^{-1}	1.63×10^{-1}

square of size 8 having a droplet of radius 2 at the center. Simulations are performed using a mesh size of 40×40. The interface curvature is numerically calculated from the LS field. Table 1 depicts the comparison of maximum magnitude of spurious velocity computed after one and 50 time steps by both the CLSVOF methods with the work of Francois et al. [2]. It is observed from the table that the magnitude of spurious velocities obtained from the algebraic CLSVOF method is slightly more than the geometric method, although these results are well validated against the work of Francois et al. [2].

4.2 Dam Break

In this problem, an initially static square water column confined in the corner of a rectangular cavity, as depicted in Fig. 1, collapses under the action of gravitational force. The parameters of the problem along with the boundary conditions are chosen according to the experimental setup of Martin and Moyce [7], shown in Fig. 1. Water is considered as the reference fluid 1 and air as the reference fluid 0. Physical properties for this problem (in SI units) are $\rho_1 = 1000$, $\rho_0 = 1.2$, $\mu_1 = 1.139 \times 10^{-2}$, and $\mu_0 = 1.78 \times 10^{-4}$. An experimental investigation was done by Martin and Moyce [7] to measure the temporal evolution of the leading edge distance of the surge front which evolves to fill the container as the water column collapses. Simulations are performed using a 128×32 uniform mesh. The result of both the CLSVOF methods along with the experimental values are presented in Fig. 2 for various non-dimensional times, $T = t\sqrt{g/a}$. Here, a is the initial width of the water column and Z is the leading edge distance from the left wall of the cavity. As compared to the experimental and numerical results in the literature [3, 9, 17], Fig. 2 shows an excellent performance of the present CLSVOF methods. Since the PLIC-CLSVOF method incorporates a sharp-interface formulation, while the interface is inherently diffused in WLIC-THINC-CLSVOF method, their performance can be better analyzed in the scenarios where the topology of the interface will undergo rapid deformation. This is evident in the next test problem.

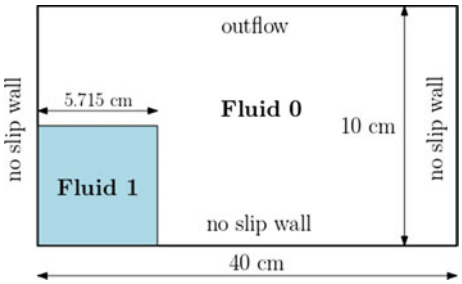

Fig. 1 Computational setup of the dam-break simulation depicting initial configuration of the interface, size of the domain, and the boundary conditions

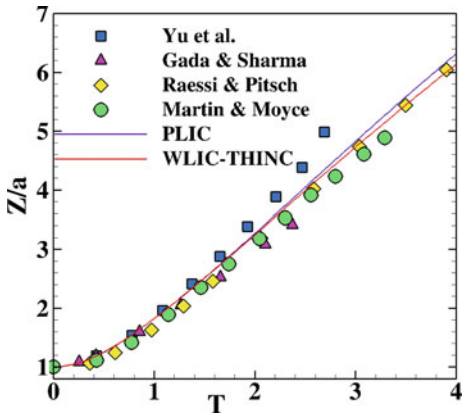

Fig. 2 Comparison of temporal evolution of the leading edge distance between present CLSVOF methods and existing experimental and numerical results

4.3 Buoyant Rise of a Bubble

A bubble, having a radius of 0.25 and centered at $(x, y) = (0.5, 0.5)$, in an initially quiescent medium, is considered here as shown in Fig. 3. The size of the computational domain and the boundary conditions are also presented in the figure. Physical properties for this problem (in SI units) are $\rho_1 = 1000$, $\rho_0 = 1$, $\mu_1 = 10$, $\mu_0 = 0.1$, $g = 0.98$, and $\sigma = 1.96$. Further, the density and viscosity ratio are 1000 and 100, respectively, which are large enough for the shape of the bubble to be considered within the skirted and dimpled ellipsoidal-cap regimes indicating that breakup may occur. Simulations are performed using a 75×150 uniform mesh and the results are presented in Fig. 4 in terms of the temporal evolution of shape of the bubble and compared with the numerical work of Hysing et al. [6]. Contrasting results are obtained from the present CLSVOF methods, as can be expected, due to their dissimilar treatment of the interface. In the PLIC-CLSVOF method, the breakup of the droplet and resulting formation of the satellite drops occur naturally due to the sharp treatment of the interface. Consequently, the obtained results validate well with the work of Hysing et al. where a similar sharp treatment of the interface was used. For the WLIC-THINC-CLSVOF method, a delayed breakup of the droplet is seen in the figure since the interface is diffused within three to four mesh cells. This results

in the formation of filament-like structures which tend to become an integral part of the bubble; thus, hampering its shape as it rises upward. To ascertain the efficacy of the CLSVOF methods quantitatively, Fig. 5 presents validation of the instantaneous rise velocity of the bubble with the work of Hysing et al. [6]. The performance of both the CLSVOF methods is in good agreement with the published results.

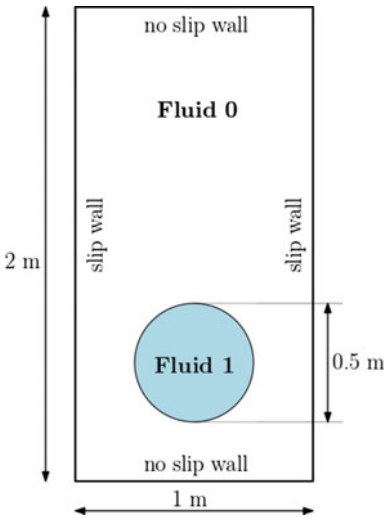

Fig. 3 Computational setup of the bubble rise simulation depicting initial configuration of the interface, size of the domain, and the boundary conditions

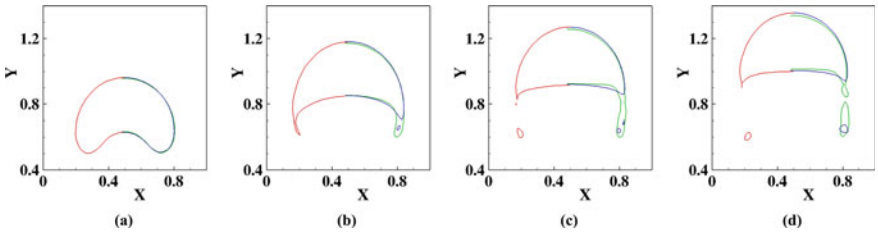

Fig. 4 Comparison of temporal evolution of the interface using the PLIC-CLSVOF (blue line) and WLIC-THINC-CLSVOF (green line) schemes at: (a) $t = 1.2$; (b) $t = 2.2$; (c) $t = 2.6$; (d) $t = 3.0$. Red line represents the work of Hysing et al. [6]

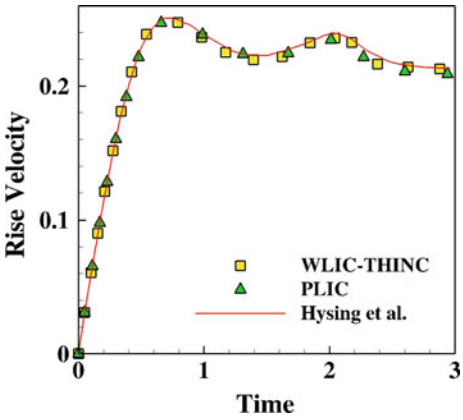

Fig. 5 Comparison of instantaneous rise velocity of the bubble between present CLSVOF methods and Hysing et al. [6]

5 Conclusions

Coupled Level Set and Volume Of Fluid (CLSVOF) methods can be broadly categorized into two types: geometric type methods and algebraic type methods. Accurate interface construction is a crucial step of the geometric methods which involves significant numerical complexity. On the other hand, in an algebraic method the interface is numerically diffused within a few mesh cells which makes them relatively straightforward to design and implement. In the present study, a framework of both geometric type Piecewise Linear Interface Calculation (PLIC) CLSVOF method and algebraic type Weighted Line Interface Calculation-Tangent of the Hyperbola for INterface Capturing (WLIC-THINC) CLSVOF method are presented along with the numerical technique for solution of the incompressible Navier–Stokes equation in a co-located grid using the balanced-force method. Relative performance of the two CLSVOF methods is studied on standard two-phase flow benchmark problems: dam break and bubble rise. The key observations are as follows.

- For the dam-break problem, similar results are obtained from both the CLSVOF methods, which are in excellent agreement with the existing experimental and numerical results.
- Simulations of the bubble rise problem, however, reveal discernible differences between the results; although validation against existing numerical results are quite satisfactory.
- This is attributed to the fact that in the PLIC-CLSVOF method, a sharp interface is maintained which can accurately mimic the droplet breakup phenomenon; and thus, can capture the dynamics precisely.
- For the WLIC-THINC-CLSVOF method, the interface is numerically diffused across three to four mesh cells causing a delayed breakup of the droplet; and thus, degrades the accuracy of the solution.

Nomenclature

$\boldsymbol{D}$	Rate of deformation tensor
F	Volume fraction
$\boldsymbol{g}$	Acceleration due to gravity (ms^{-2})
k	Interface curvature (ms^{-1})
P	Piezometric pressure (Nm^{-2})
$\boldsymbol{u}$	Velocity vector (ms^{-1})
t	Time (s)
β	Interface thickness parameter–
Γ	Advected property
σ	Surface tension coefficient (Nm^{-1})
φ	Level set
χ	Characteristic function
Ω	Interface weights
(-)	Volume-averaged quantity

References

1. Arrufat T, Crialesi-Esposito M, Fuster D, Ling Y, Malan L, Pal S, Scardovelli R, Tryggvason G, Zaleski S (2021) A mass-momentum consistent, volume-of-fluid method for incompressible flow on staggered grids. Comput Fluids 215:104785
2. Francois MM, Cummins SJ, Dendy ED, Kothe DB, Sicilian JM, Williams MW (2006) A balanced-force algorithm for continuous and sharp interfacial surface tension models within a volume tracking framework. J Comput Phys 213(1):141–173
3. Gada VH, Sharma A (2011) On a novel dual-grid level-set method for two-phase flow simulation. Numer Heat Transf, Part B: Fundamentals 59(1):26–57
4. Hirt CW, Nichols BD (1981) Volume of fluid (VOF) method for the dynamics of free boundaries. J Comput Phys 39(1):201–225
5. Hong W-L, Walker DT (2000) Reynolds-averaged equations for free-surface flows with application to high-Froude-number jet spreading. J. Fluid Mech 417:183–209
6. Hysing S-R, Turek S, Kuzmin D, Parolini N, Burman E, Ganesan S, Tobiska L (2009) Quantitative benchmark computations of two-dimensional bubble dynamics. Int J Numer Meth Fluids 60(11):1259–1288
7. Martin JC, Moyce WJ (1952) Part IV. An experimental study of the collapse of liquid columns on a rigid horizontal plane. Philos. Trans. Roy. Soc. London A 244:312–324
8. Pilliod Jr JE, Puckett EG (2004) Second-order accurate volume-of-fluid algorithms for tracking material interfaces. J Comput Phys 199(2):465–502
9. Raessi M, Pitsch H (2012) Consistent mass and momentum transport for simulating incompressible interfacial flows with large density ratios using the level set method. Comput Fluids 63:70–81
10. Rudman M (1997) Volume-tracking methods for interfacial flow calculations. Int J Numer Meth Fluids 24(7):671–691
11. Saad Y, Kesheng W (1996) DQGMRES: a direct quasi-minimal residual algorithm based on incomplete orthogonalization. Numer Linear Algebra with Appl 3(4):329–343
12. Son G, Hur N (2002) A coupled level set and volume-of-fluid method for the buoyancy-driven motion of fluid particles. Numer Heat Transfer: Part B: Fundament 42(6):523–542

13. Sussman M, Puckett EG (2000) A coupled level set and volume-of-fluid method for computing 3D and axisymmetric incompressible two-phase flows. J Comput Phys 162(2):301–337
14. Sussman M, Smereka P, Osher S (1994) A level set approach for computing solutions to incompressible two-phase flow. J Comput Phys 114(1):146–159
15. Xiao F, Honma Y, Kono T (2005) A simple algebraic interface capturing scheme using hyperbolic tangent function. Int J Numer Meth Fluids 48(9):1023–1040
16. Yokoi K (2007) Efficient implementation of THINC scheme: a simple and practical smoothed VOF algorithm. J Comput Phys 226(2):1985–2002
17. Yu C-H, Wen HL, Gu ZH, An RD (2019) Numerical simulation of dam-break flow impacting a stationary obstacle by a CLSVOF/IB method. Commun Nonlinear Sci Numer Simul 79:104934
18. Zhao H (2005) A fast sweeping method for Eikonal equations. Math Comput 74(250):603–627